

Polytropic stars in bootstrapped Newtonian gravity

Roberto Casadio^{1,2,*} and Octavian Micu^{3,†}

¹*Dipartimento di Fisica e Astronomia, Università di Bologna via Irnerio 46, 40126 Bologna, Italy*

²*I.N.F.N., Sezione di Bologna, I.S. FLAG viale B. Pichat 6/2, 40127 Bologna, Italy*

³*Institute of Space Science, Bucharest, Romania P.O. Box MG-23,
RO-077125 Bucharest-Magurele, Romania*



(Received 3 July 2020; accepted 21 October 2020; published 19 November 2020)

We study self-gravitating stars in the bootstrapped Newtonian picture for polytropic equations of state. We consider stars that span a wide range of compactness values. Both matter density and pressure are sources of the gravitational potential. Numerical solutions show that the density profiles can be well approximated by Gaussian functions. Later we assume Gaussian density profiles to investigate the interplay between the compactness of the source, the width of the Gaussian density profile and the polytropic index. We also dedicate a section to comparing the pressure and density profiles of the bootstrapped Newtonian stars to the corresponding general relativistic solutions. We also point out that no Buchdahl limit is found, which means that the pressure can in principle support a star of arbitrarily large compactness. In fact, we find solutions representing polytropic stars with compactness above the Buchdahl limit.

DOI: [10.1103/PhysRevD.102.104058](https://doi.org/10.1103/PhysRevD.102.104058)

I. INTRODUCTION AND MOTIVATION

One of the most striking features of the strong gravity regime in general relativity is that, once a trapping surface appears, singularity theorems require an object to collapse all the way into a region of infinite density surrounded by a black hole geometry [1]. Static black hole spacetimes are however problematic in this classical description, since pointlike sources are mathematically incompatible with the Einstein equations [2]. One would therefore hope that quantum physics solves this fundamental puzzle in the description of self-gravitating objects, the same way it removes the ultraviolet catastrophe and makes the hydrogen atom stable. Given the strong experimental constraints on possible deviations from general relativity, quantum effects can only become significant in the strong field regime, where perturbative methods hardly apply and matter likely requires physics beyond the standard model as well [3]. In particular, whether the scale at which quantum departures from general relativity become appreciable is significantly large to affect the description of compact astrophysical objects remain a key physical question.

In light of the above observations, in Refs. [4,5] we studied solutions of an effective equation for the gravitational potential of a static source which contains a gravitational self-interaction term besides the usual Newtonian coupling with the matter density. Following an idea from

Ref. [6], the self-interaction term was derived in details from a Fierz-Pauli Lagrangian in Ref. [7], and it could therefore be viewed as the first step in the perturbative reconstruction of general relativity (see e.g., Refs. [8]). However, since the equation for the potential was solved nonperturbatively [4,5], it could also be conjectured that this “bootstrapped” Newtonian gravity effectively describes the (mean field) quantum gravitational potential of extremely compact objects after the break-down of classical general relativity [9,10]. Moreover, we found no equivalent of the Buchdahl limit [11], a result implying that matter pressure (possibly of quantum origin) could support sources of arbitrarily large compactness

$$X \equiv \frac{G_N M}{R}, \quad (1.1)$$

where R is the radius and M the ADM-like [12] mass [13] of the source.¹

Like in Refs. [4,5], we shall just consider (static) spherically symmetric systems, so that all quantities depend only on the radial coordinate r , but the density profile is not restricted to be uniform. We shall begin by assuming that the matter density $\rho = \rho(r)$ and pressure $p = p(r)$ satisfy a polytropic equation of state and determine the density profile numerically for different values of the compactness (and of the polytropic parameters). This analysis will show that the equilibrium configurations

*casadio@bo.infn.it

†octavian.micu@spacescience.ro

¹In this paper we use units with $c = 1$, and always display the Newton constant G_N explicitly.

closely resemble Gaussian distributions. Therefore, we shall also study Gaussian density profiles analytically and determine *a posteriori* the compatible polytropic parameters.

The paper is organized as follows: in Sec. II, we briefly review the bootstrapped Newtonian picture; Sec. III is dedicated to the investigation of the model within the further assumption of a polytropic equation of state for the matter source and to finding numerical solutions for the density profile; that is followed in Sec. IV by an in depth analysis of Gaussian density profiles and comparison with general relativity in Sec. V; finally we comment about our results and possible outlooks in Sec. VI.

II. BOOTSTRAPPED THEORY FOR THE GRAVITATIONAL POTENTIAL

From Ref. [7], we recall that the non-linear equation for the potential $V = V(r)$ describing the gravitational pull on test particles generated by a matter density $\rho = \rho(r)$ can be obtained starting from the Newtonian Lagrangian

$$L_N[V] = -4\pi \int_0^\infty r^2 dr \left[\frac{(V')^2}{8\pi G_N} + \rho V \right], \quad (2.1)$$

where $f' \equiv df/dr$, and the corresponding field equation is the Poisson equation

$$r^{-2}(r^2 V')' \equiv \Delta V = 4\pi G_N \rho \quad (2.2)$$

for the Newtonian potential $V = V_N$. We can then include the effects of gravitational self-interaction by noting that the Hamiltonian

$$H_N[V] = -L_N[V] = 4\pi \int_0^\infty r^2 dr \left(-\frac{V \Delta V}{8\pi G_N} + \rho V \right), \quad (2.3)$$

computed on-shell by means of Eq. (2.2), yields the Newtonian potential energy

$$\begin{aligned} U_N(r) &= 2\pi \int_0^r \bar{r}^2 d\bar{r} \rho(\bar{r}) V(\bar{r}) \\ &= -\frac{1}{2G_N} \int_0^r \bar{r}^2 d\bar{r} [V'(\bar{r})]^2, \end{aligned} \quad (2.4)$$

where we used Eq. (2.2) and then integrated by parts discarding boundary terms. One can view the above U_N as given by the interaction of the matter distribution enclosed in a sphere of radius r with the gravitational field. Following Ref. [6] (see also Refs. [14]), we then define a self-gravitational source proportional to the gravitational energy U_N per unit volume, that is

$$J_V \simeq \frac{dU_N}{dV} = -\frac{[V'(r)]^2}{2\pi G_N}. \quad (2.5)$$

In Ref. [5], we found that the pressure p becomes very large for compact sources with $X \gtrsim 1$, and we must therefore add a corresponding potential energy U_B such that

$$p = -\frac{dU_B}{dV}. \quad (2.6)$$

Since the latter contribution just adds to ρ , it can be easily included by simply shifting $\rho \rightarrow \rho + q_c p$, where q_c is a positive constant which allows us to implement the non-relativistic limit formally as $q_c \rightarrow 0$. Upon including these new source terms, and the analogous higher order term $J_\rho = -2V^2$ which couples with the matter source, we obtain the total Lagrangian [7]

$$\begin{aligned} L[V] &= L_N[V] - 4\pi \int_0^\infty r^2 dr [q_\Phi J_V V + q_\Phi J_\rho (\rho + q_c p)] \\ &= -4\pi \int_0^\infty r^2 dr \left[\frac{(V')^2}{8\pi G_N} (1 - 4q_\Phi V) \right. \\ &\quad \left. + (\rho + q_c p) V (1 - 2q_\Phi V) \right], \end{aligned} \quad (2.7)$$

where the positive parameter q_Φ plays the role of a coupling constant for the graviton current J_V and the higher-order matter current J_ρ . The associated effective Hamiltonian is simply given by

$$H[V] = -L[V]. \quad (2.8)$$

Finally, the Euler-Lagrange equation for V is given by

$$\Delta V = 4\pi G_N (\rho + q_c p) + \frac{2q_\Phi (V')^2}{1 - 4q_\Phi V} \quad (2.9)$$

and the conservation equation that determines the pressure reads

$$p' = -V'(\rho + q_c p). \quad (2.10)$$

The exact Newtonian equations are then recovered by taking the nonrelativistic limit as $q_c \rightarrow 0$ and switching off the graviton self-interaction with $q_\Phi \rightarrow 0$. It is important to remark that the couplings q_Φ and q_c do not need to be small. In fact, the closest results to general relativity are expected to occur for $q_\Phi \simeq q_c \simeq 1$ [4].

III. POLYTROPIC STARS

In Refs. [4,5,7,13], the effects of the gravitational self-interaction, encoded by the term proportional to q_Φ in the field equation (2.9), were analyzed by considering simple sources, characterized by a homogeneous matter density $\rho = \rho_0$ and different values of the compactness X . One of the main results is that, for a flat density profile, the outer mass parameter M is always larger than the proper mass

$$M_0 = m(R) = 4\pi \int_0^R r^2 dr \rho(r). \quad (3.1)$$

This is in agreement with the fact that M should also account for the (positive) pressure required to ensure equilibrium, with M approaching M_0 for smaller and smaller compactness X [4].

We now want to study more realistic matter distributions, for which we expect that the degeneracy pressure is the main component counteracting the gravitational pull, like in neutron stars and white dwarfs. For this purpose, we will assume a polytropic equation of state [15]

$$p(r) = \gamma \rho^n(r) = \tilde{\gamma} \rho_0 \left[\frac{\rho(r)}{\rho_0} \right]^n, \quad (3.2)$$

with n and $\tilde{\gamma}$ positive dimensionless parameters, and $\rho_0 \equiv \rho(0)$ is used as a reference density. Moreover, we shall also assume the surface pressure vanishes, $p_R \equiv p(R) = 0$, which then implies that $\rho_R \equiv \rho(R) = 0$.

The relevant solutions for the density profile will have to lead to a potential which satisfies the regularity condition in the center

$$V'_{\text{in}}(0) = 0 \quad (3.3)$$

and be smooth across the surface $r = R$, that is

$$V_{\text{in}}(R) = V_{\text{out}}(R) \equiv V_R \quad (3.4)$$

$$V'_{\text{in}}(R) = V'_{\text{out}}(R) \equiv V'_R, \quad (3.5)$$

where we defined $V_{\text{in}} = V(0 \leq r \leq R)$ and $V_{\text{out}} = V(R \leq r)$. The consistency of these two conditions with Eq. (3.2) will be thoroughly analyzed below after we recall the outer vacuum solution.

A. Outer vacuum solution

Outside the source, we have $\rho = p = 0$ and Eq. (2.10) is trivially satisfied. Equation (2.9) reads

$$\Delta V = \frac{2q_\Phi (V')^2}{1 - 4q_\Phi V}, \quad (3.6)$$

which is exactly solved by

$$V_{\text{out}} = \frac{1}{4q_\Phi} \left[1 - \left(1 + \frac{6q_\Phi G_N M}{r} \right)^{2/3} \right]. \quad (3.7)$$

where two integration constants were fixed by requiring the expected Newtonian behavior in terms of the ADM-like mass M for large r . In fact, for large r , we have

$$V_{\text{out}} \simeq -\frac{G_N M}{r} + q_\Phi \frac{G_N^2 M^2}{r^2} - q_\Phi^2 \frac{8G_N^3 M^3}{3r^3}, \quad (3.8)$$

which displays the expected post-Newtonian term of order G_N^2 for $q_\Phi = 1$ [7].

For sufficiently large X , the outer potential gives rise to a ‘‘Newtonian’’ horizon of radius [4]

$$r_H \simeq 1.4 G_N M, \quad (3.9)$$

precisely where $2V_{\text{out}}(r_H) = -1$. In this work, we shall therefore assume $X < 0.7$ in order to avoid this feature.

From Eq. (3.7), we also obtain

$$V_R = V_{\text{out}}(R) = \frac{1}{4q_\Phi} [1 - (1 + 6q_\Phi X)^{2/3}], \quad (3.10)$$

and

$$RV'_R = RV'_{\text{out}}(R) = \frac{X}{(1 + 6q_\Phi X)^{1/3}}, \quad (3.11)$$

which we will often use since they appear in the boundary conditions (3.4) and (3.5).

B. The inner pressure and potential

The conservation equation (2.10) for the polytropic equation of state (3.2) immediately allows one to find the derivative of the potential

$$V' = -\frac{n\gamma\rho'}{q_c\gamma\rho + \rho^{2-n}} = -\frac{n\tilde{\gamma}\rho'}{q_c\tilde{\gamma}\rho + \rho_0^{n-1}\rho^{2-n}}. \quad (3.12)$$

The regularity condition (3.3) then requires $\rho'(0) = 0$, which can hold for any $\rho_0 \equiv \rho(0) > 0$. For $n \neq 1$, the above equation yields

$$\begin{aligned} V &= \beta - \frac{n}{(n-1)q_c} \ln(1 + q_c\gamma\rho^{n-1}) \\ &= \beta - \frac{n}{(n-1)q_c} \ln \left[1 + q_c\tilde{\gamma} \left(\frac{\rho}{\rho_0} \right)^{n-1} \right], \end{aligned} \quad (3.13)$$

where β is an integration constant. On the other hand, for $n = 1$ the constant $\gamma = \tilde{\gamma}$ is dimensionless, and we find the simpler solution

$$V = \beta - \frac{\gamma}{q_c\gamma + 1} \ln \left(\frac{\rho}{\rho_0} \right). \quad (3.14)$$

We remark that Eqs. (3.13) and (3.14) reproduce the Newtonian behavior in the nonrelativistic limit $q_c \rightarrow 0$. Moreover, the above expressions for V and V' evaluated at $r = R$ must equal the respective outer values (3.10) and (3.11), which only depend on M and R , but not on any equation of state. Let us then analyze in details under which

conditions the equation of state (3.2) is compatible with the continuity of the potential and its derivative.

For $n > 1$, continuity of the potential (3.13) across $r = R$ simply fixes the integration constant

$$\beta = V_R, \quad (3.15)$$

where we used $\rho_R = 0$. Values of n outside this range must however be excluded.² In fact, for $n = 1$, the solution (3.14) diverges positively and so does Eq. (3.13) for $0 < n \leq 1$.

Moreover, in the allowed range $n > 1$, continuity of the derivative of the potential demand

$$\frac{V'_R}{n\gamma} = -\lim_{r \rightarrow R} \left(\frac{\rho'}{\rho^{2-n}} \right) \equiv \frac{Y}{n\gamma R} > 0, \quad (3.16)$$

which implies that $\rho' \sim -\rho^{2-n}$ for $r \rightarrow R$. It is important to remark that this condition holds irrespectively of the value of q_c , precisely because $n > 1$ implies that the term $q_c \rho$ vanishes faster than ρ^{2-n} . For $1 < n < 2$, both ρ and ρ' must then vanish at the star surface. For $n = 2$, the derivative ρ' must be finite there, whereas for $n > 2$ it must diverge (negatively) for $r \rightarrow R$ from inside. This latter behavior could be roughly approximated with a step discontinuity at the surface of the star. We then remark that the text-book cases of relativistic ($n = 4/3$) and nonrelativistic ($n = 5/3$) fermions belong to the range $1 < n < 2$.

For $n > 1$, Eq. (3.5) now reads

$$Y = \frac{X}{(1 + 6q_\Phi X)^{1/3}}, \quad (3.17)$$

which can be used to determine the compactness X from the behavior of the density at the star surface. Of the three solutions for X , only one is real and positive and reads

$$\frac{X_s}{Y} = \frac{2^{1/3}(1 + \sqrt{1 - 32q_\Phi^3 Y^3})^{2/3} + 4q_\Phi Y}{2^{2/3}(1 + \sqrt{1 - 32q_\Phi^3 Y^3})^{1/3}}, \quad (3.18)$$

which holds for all values of $Y > 0$. We note that $X_s = Y$ for $q_\Phi = 0$, corresponding to the Newtonian theory, and an expansion for small Y yields

$$\frac{X_s}{Y} \simeq 1 + 2q_\Phi Y + \frac{8}{3} q_\Phi^3 Y^3. \quad (3.19)$$

This shows that the compactness is always larger in the bootstrapped theory than it would be in the Newtonian case for the same Y (see Fig. 1 for a plot of the exact result).

²Eq. (3.2) is often written as $p = \gamma \rho^{1+1/n'}$, with $n' > 0$ in the astrophysical literature.

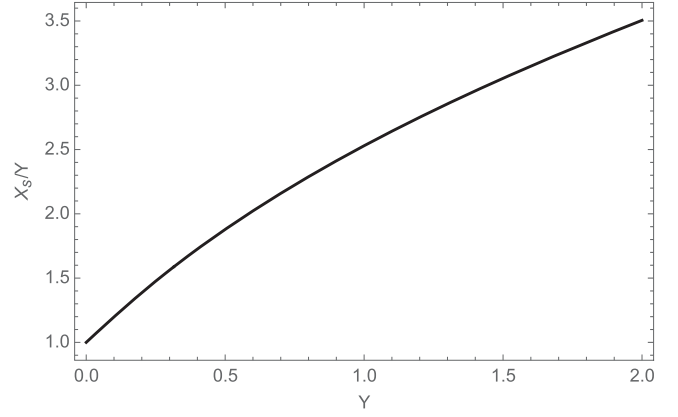


FIG. 1. Compactness in Eq. (3.18) with $q_\Phi = 1$.

Finally, we can determine more explicitly the boundary behavior (at $r \lesssim R$) of the density, which is governed by the equation

$$\gamma n R \frac{\rho'}{\rho^{2-n}} \simeq -Y, \quad (3.20)$$

with the conditions that $\rho_R = 0$ and $n > 1$. For $Y > 0$, we then find

$$\begin{aligned} \rho &\simeq \left[\frac{n-1}{n} \left(1 - \frac{r}{R} \right) \frac{Y}{\gamma} \right]^{1/(n-1)} \\ &\simeq \left[\frac{n-1}{n\gamma} \left(1 - \frac{r}{R} \right) \frac{X}{(1 + 6q_\Phi X)^{1/3}} \right]^{1/(n-1)}. \end{aligned} \quad (3.21)$$

Upon expanding for small compactness, one then obtains

$$\rho \simeq \left[\frac{n-1}{n\gamma} \left(1 - \frac{r}{R} \right) X \right]^{1/(n-1)} \left(1 - \frac{2q_\Phi X}{n-1} \right), \quad (3.22)$$

which shows that the density near the surface must be smaller in the bootstrapped theory than it is in the Newtonian theory for a star of given (small) compactness. We remark once more that this result is independent of the nonrelativistic limit $q_c \rightarrow 0$ because relativistic corrections proportional to q_c are subleading near the surface of the source for $n > 1$.

To summarize, we have obtained the general behavior of the density required by the equation of state (3.2) to be compatible with a smooth potential across the surface. We remark that one could relax the condition (3.5) on the derivative of the potential in order to allow for a (vanishingly thin) solid crust. In Sec. IV, we shall employ an analytical approximation for the density inside the whole star and consider in particular the text-book equations of state for relativistic and non-relativistic fermions, so that $1 < n < 2$ and $\rho'(R) = \rho(R) = 0$. Before that, we will tackle the problem numerically.

C. Density equation and numerical solutions

For the cases of interest, the potential is expressed exactly in terms of the density by Eq. (3.13) with $1 < n < 2$ and β given in Eq. (3.15). This makes it more convenient to rewrite the second order ordinary differential equation (2.9) inside the source as an equation for the density $\rho = \rho(r)$, with the two boundary conditions

$$\rho(R) = 0 \quad (3.23)$$

$$\rho'(0) = 0. \quad (3.24)$$

Furthermore, in order to solve for the density numerically, we shall introduce dimensionless variables by using R

as the unit of length. For instance, we write the radial coordinate $r = R\bar{r}$ and note that the compactness X is already dimensionless. Likewise, the dimensionless density $\bar{\rho}$ is defined by

$$G_{\text{NP}} = \frac{X\bar{\rho}}{R^2} \quad (3.25)$$

and the polytropic equation of state (3.2) yields

$$G_{\text{NP}} = \frac{\bar{\gamma}}{R^2} (X\bar{\rho})^n, \quad (3.26)$$

where the dimensionless $\bar{\gamma}$ should not be confused with $\tilde{\gamma}$.³ The equation for the dimensionless density then reads

$$\frac{\partial_{\bar{r}}}{\bar{r}^2} \left[\frac{n\bar{\gamma}\bar{r}^2 \partial_{\bar{r}}(\ln \bar{\rho})}{q_c \bar{\gamma} + (X\bar{\rho})^{1-n}} \right] = -4\pi X \bar{\rho} [1 + q_c \bar{\gamma} (X\bar{\rho})^{n-1}] - \frac{2q_{\Phi} n^2 (n-1) \bar{\gamma}^2 [\partial_{\bar{r}}(\ln \bar{\rho})]^2}{[q_c \bar{\gamma} + (X\bar{\rho})^{1-n}]^2 \{(n-1)(1-4q_{\Phi} V_R) + 4q_{\Phi} n q_c^{-1} \ln [1 + q_c \bar{\gamma} (X\bar{\rho})^{n-1}]\}}, \quad (3.27)$$

in which we note that V_R is given in Eq. (3.10) and is a function of X only.

We have performed a preliminary numerical analysis of the above equation and boundary conditions for $q_c = q_{\Phi} = 1$. We also want to avoid values of the compactness corresponding to Newtonian black holes corresponding to $X \gtrsim 0.7$ (as discussed in Sec. III A). The relevant parameter space is thus given by $0 < X < 0.7$, $1 < n < 2$ and $\bar{\gamma} > 0$, a complete analysis of which would require extensive numerical works beyond our present scope. A first interesting result is that, for fixed values of n and $\bar{\gamma}$, solutions only exist for certain ranges of X , similarly to the case of general relativity. Examples of high compactness are given in Figs. 2 for $n = 5/3$, from which we see that the larger X , the flatter the dimensionless profile of $\bar{\rho}$, whereas the fully dimensional density grows larger in the centre and so does the pressure. Another preliminary result is that solutions are found for lower values of X only by suitably lowering $\bar{\gamma}$ correspondingly. Examples for the same $n = 5/3$ are given in Figs. 3. Finally, we have found that smaller values of n produce more peaked profiles, like is shown for $n = 4/3$ in Fig. 4.

In all the case we have been able to solve Eq. (3.27), the density profile can be rather closely approximated with a Gaussian function. In the following, we shall therefore take the opposite perspective and try to determine the polytropic parameters compatible with given Gaussian profiles.

IV. GAUSSIAN DENSITY PROFILES

We start from assuming the density profile of the self-gravitating object is given by

$$\rho = \begin{cases} \rho_0 e^{-\frac{r^2}{b^2 R^2}}, & r \leq R \\ 0, & r > R. \end{cases} \quad (4.1)$$

Since $\rho_R \equiv \rho(R) > 0$, the density (4.1) contains a steplike discontinuity at $r = R$, like the uniform profiles analyzed in Refs. [4,5]. Of course, such a discontinuity is incompatible with a polytropic equation of state if one continues to require vanishing pressure at the surface. However, we can set the central density ρ_0 and the width b such that

$$-\lim_{r \rightarrow R} \left(\frac{\rho'}{\rho^{2-n}} \right) = \frac{\rho_0^{n-1}}{b^2} e^{-(n-1)/b^2} = \frac{Y}{2\gamma}, \quad (4.2)$$

and note that for $b \ll 1$, we can have $\rho_R \ll \rho_0$. A mild discontinuity of this form could be tolerable, for instance, by assuming that the surface of the object is covered by a thin solid crust with a tension that balances the non-vanishing pressure.

Technically, the discontinuity could also be removed completely by subtracting the constant ρ_R from the profile (4.1) for $r \leq R$. In so doing, one would however introduce more serious obstacles with the continuity of the first derivative of the potential, since the denominator in Eq. (3.12) would then vanish and V' correspondingly diverge. We therefore find it still preferable to allow for a (slight) discontinuity at the surface with $\rho_R \ll \rho_0$. It needs to be mentioned that, due to this discontinuity, Eq. (3.15) for β also gets modified, as will be seen later.

³We note that ρ_0 is not a convenient parameter here since the central density cannot be set freely.

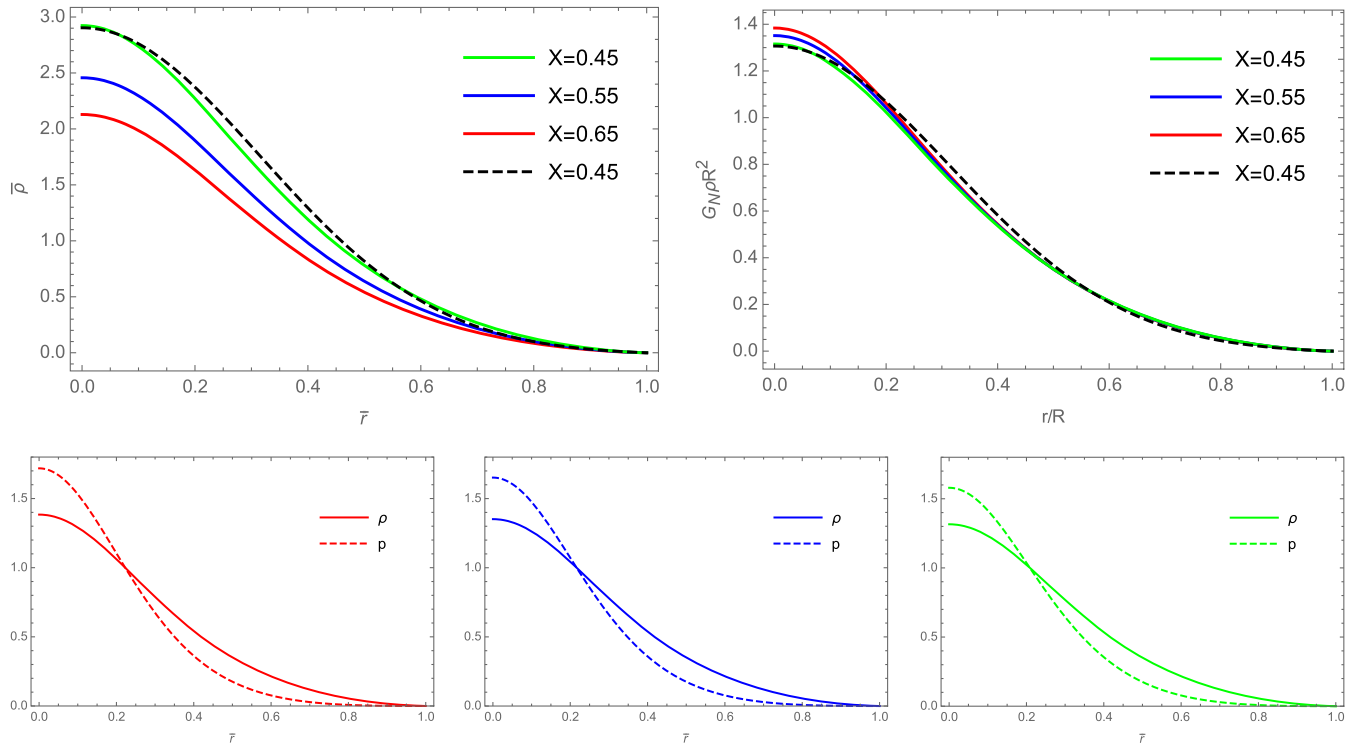


FIG. 2. Upper panels: density profile calculated numerically for $\tilde{\gamma} = 1$, $n = 5/3$ (solid lines) and Gaussian approximation (dashed line) for the lowest compactness (left panel: dimensionless quantities; right panel: dimensionful quantities). Lower panels: density (solid lines) and pressure (dashed lines) for the cases in the upper panels.

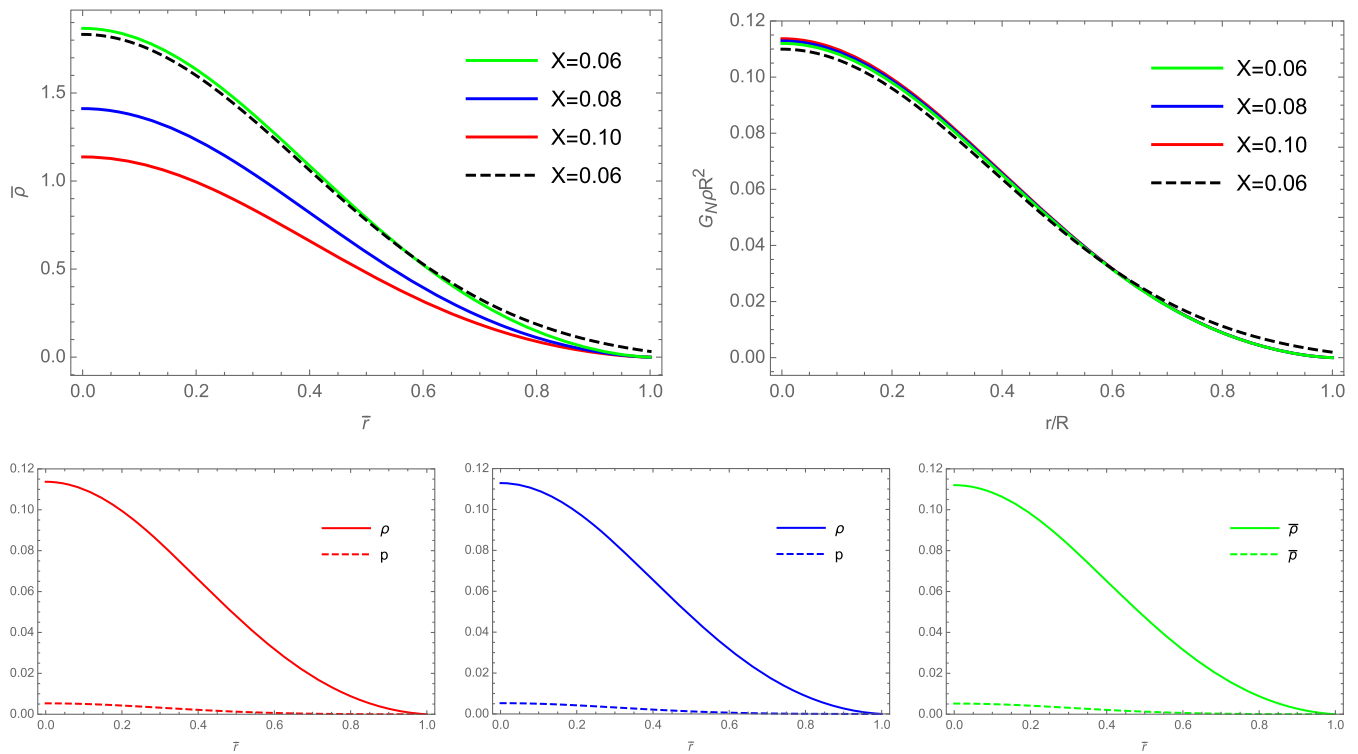


FIG. 3. Upper panels: density profile calculated numerically for $\tilde{\gamma} = 0.2$, $n = 5/3$ (solid lines) and Gaussian approximation (dashed line) for the lowest compactness (left panel: dimensionless quantities; right panel: dimensionful quantities). Lower panels: density (solid lines) and pressure (dashed lines) for the cases in the upper panels.

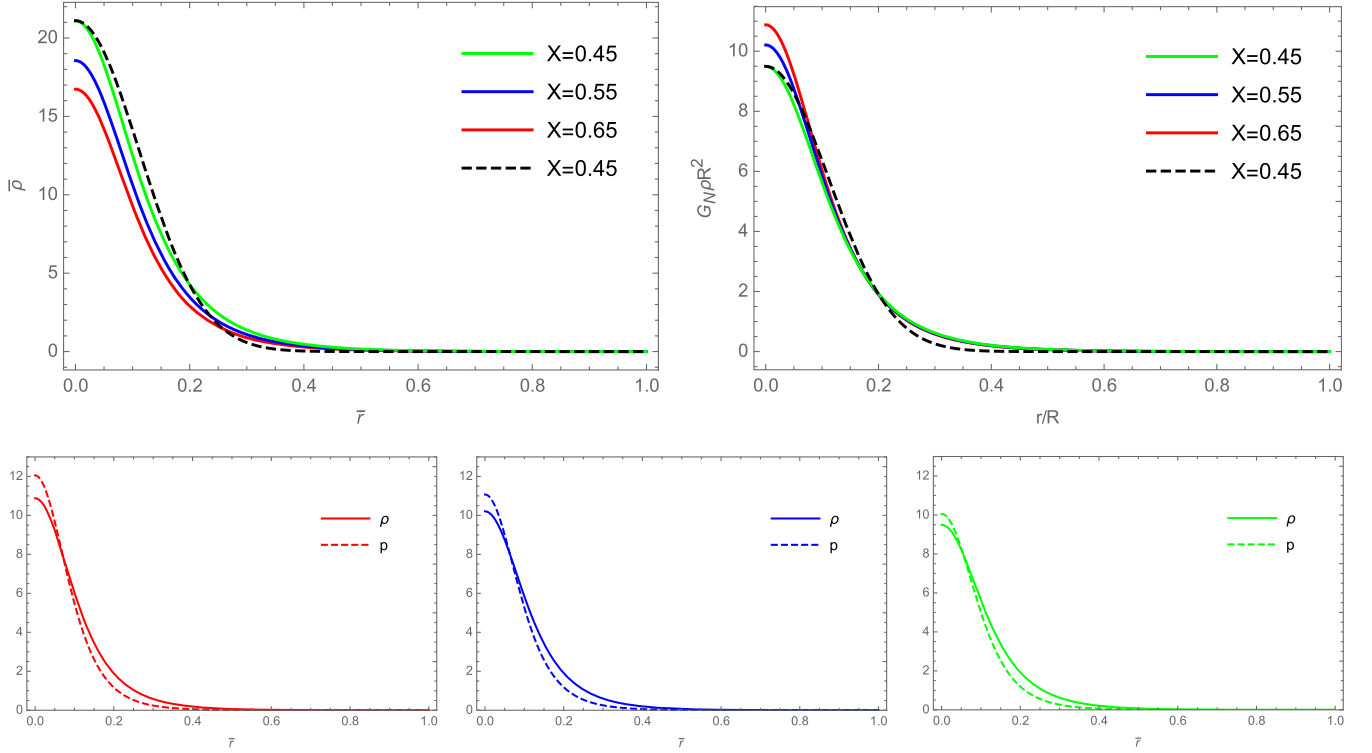


FIG. 4. Upper panels: density profile calculated numerically for $\tilde{\gamma} = 0.5$, $n = 4/3$ (solid lines) and Gaussian approximation (dashed line) for the lowest compactness (left panel: dimensionless quantities; right panel: dimensionful quantities). Lower panels: density (solid lines) and pressure (dashed lines) for the cases in the upper panels.

Starting from Eqs. (3.12) and (3.13), and using the two boundary conditions (3.4) and (3.5), we can determine both β and γ as functions of the other remaining parameters. Continuity of the first derivative of the potential (3.5) allows us to express one of the parameters which determine the equation of state, $\tilde{\gamma}$ (respectively γ), in terms of the polytropic index n , the compactness X and the width b , as

$$\tilde{\gamma} = \frac{X e^{(n-1)/b^2}}{\frac{2n}{b^2} (1 + 6q_\Phi X)^{1/3} - q_c X}. \quad (4.3)$$

Using the boundary condition (3.4), we then determine

$$\begin{aligned} \beta &= V_R + \frac{n}{(n-1)q_c} \ln [1 + q_c \tilde{\gamma} e^{(1-n)/b^2}] \\ &= V_R + \frac{n}{(n-1)q_c} \ln \left[1 + \frac{q_c X}{\frac{2n}{b^2} (1 + 6q_\Phi X)^{1/3} - q_c X} \right]. \end{aligned} \quad (4.4)$$

These expressions for $\tilde{\gamma}$ and β can be substituted into the field equation (2.9), but no exact analytical expression can then be found for the remaining parameters. We can proceed by expanding both sides of Eq. (2.9) in power series around $r = 0$. Equating the lowest order terms yields

$$\begin{aligned} \rho_0 &= \frac{3n\tilde{\gamma}}{2\pi b^2 G_N R^2 (1 + q_c \tilde{\gamma})^2} \\ &= \frac{3nX e^{(n+1)/b^2} [\frac{2n}{b^2} (1 + 6q_\Phi X)^{1/3} - q_c X]}{2\pi b^2 G_N R^2 [e^{n/b^2} q_c X + e^{1/b^2} (\frac{2n}{b^2} (1 + 6q_\Phi X)^{1/3} - q_c X)]^2}, \end{aligned} \quad (4.5)$$

from which we can write

$$\begin{aligned} \rho &= \frac{3n\tilde{\gamma} e^{-r^2/b^2 R^2}}{2\pi b^2 G_N R^2 (1 + q_c \tilde{\gamma})^2} \\ &= \frac{3nX e^{(n+1-r^2/R^2)/b^2} [\frac{2n}{b^2} (1 + 6q_\Phi X)^{1/3} - q_c X]}{2\pi b^2 G_N R^2 [e^{n/b^2} q_c X + e^{1/b^2} (\frac{2n}{b^2} (1 + 6q_\Phi X)^{1/3} - q_c X)]^2}. \end{aligned} \quad (4.6)$$

We also notice that both ρ_0 and $\tilde{\gamma}$ must be positive, which holds if

$$n > \frac{q_c b^2 X}{2(1 + 6q_\Phi X)^{1/3}} \equiv n_{\min}. \quad (4.7)$$

This is a non-trivial lower bound for the polytropic index depending on the compactness and width of the density profile. Since we expect $1 < n < 2$, the compactness and width must satisfy

$$8(1 + 6q_\Phi X) < q_c^3 b^6 X^3 < 64(1 + 6q_\Phi X), \quad (4.8)$$

otherwise no n exists and the star cannot be described by polytropic matter. The range of values for the compactness X that will be considered further covers all possible types of sources, from very low densities to objects on the brink of contracting behind the event horizon and becoming black holes, as discussed in Sec. III A. The lower bound n_{\min} from Eq. (4.7) is shown in Fig. 5 for $q_c = q_\Phi = 1$ and $0 < X < 0.7$. The entire range $1 < n < 2$ is clearly allowed.

The ADM mass M and the proper mass M_0 of the star are generally different. The proper mass is obtained from the volume integral of the density in Eq. (3.1), which, for our Gaussian distributions, reads

$$M_0 = \frac{3nXR e^{n/b^2} [\frac{2n}{b^2} (1 + 6q_\Phi X)^{1/3} - q_c X] [e^{1/b^2} \sqrt{\pi} \text{Erf}(\frac{1}{b}) - 2]}{2G_N [e^{n/b^2} q_c X + e^{1/b^2} (\frac{2n}{b^2} (1 + 6q_\Phi X)^{1/3} - q_c X)]^2}, \quad (4.9)$$

where the dependence on the ADM mass is hidden in the compactness X . This allows us to calculate the ratio

$$\frac{M_0}{M} = \frac{3n e^{n/b^2} [\frac{2n}{b^2} (1 + 6q_\Phi X)^{1/3} - q_c X] [e^{1/b^2} \sqrt{\pi} \text{Erf}(\frac{1}{b}) - 2]}{2 [e^{n/b^2} q_c X + e^{1/b^2} (\frac{2n}{b^2} (1 + 6q_\Phi X)^{1/3} - q_c X)]^2}. \quad (4.10)$$

Finally, we can rewrite the potential from Eq. (3.13) as

$$V_b = \frac{n}{(n-1)q_c} \ln \left[\frac{\frac{2n}{b^2} (1 + 6q_\Phi X)^{1/3}}{\frac{2n}{b^2} (1 + 6q_\Phi X)^{1/3} + q_c X (e^{(n-1)(1-r^2/R^2)/b^2} - 1)} \right] + \frac{1}{4q_\Phi} [1 - (1 + 6q_\Phi X)^{2/3}], \quad (4.11)$$

where the suffix b is to remark that this analytical expression stems from a density which only solves the polytropic equation of state approximately due to $\rho_R > 0$.

Besides the compactness, this potential still depends on two parameters: the width b of the density distribution and the polytropic index n from the equation of state. Due to the complexity of the field equation (2.9), we must rely on some approximate method in order to study the dependence of the equation of state on the width of the density profile. To this purpose, we write the potential as

$$V = V_b + W, \quad (4.12)$$

where V is the exact solution to Eq. (2.9) and the difference W with respect to the analytical expression (4.11) can be computed numerically. The preferred values, or ranges of values, for the polytropic index n will then be obtained by minimizing the relative error W/V for given values of the width b and compactness X . In particular, we will perform the analysis for three values of the compactness: small compactness $X = 0.01$, intermediate compactness $X = 0.1$ and large compactness $X = 0.7$. Considering the discussion of the discontinuity at the surface from the beginning of this

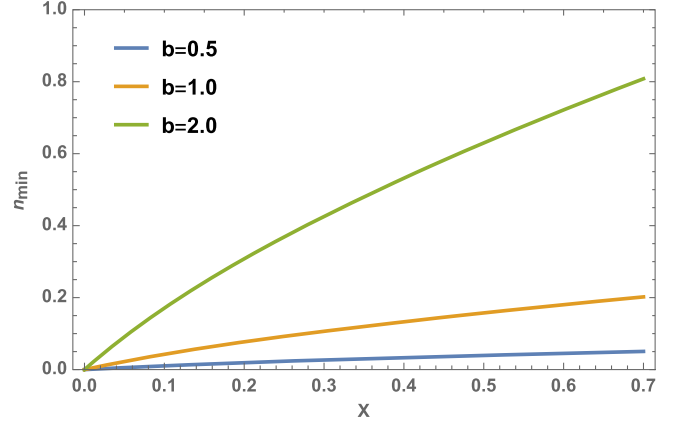


FIG. 5. Minimum value of the polytropic index n for $q_c = q_\Phi = 1$.

section, and the numerical results from the previous section, we are also interested in cases with $\rho_0 \gg \rho_R$. Therefore we will perform simulations for $b = 0.5$, for which $\rho_R/\rho_0 \simeq 1.8\%$. In anticipation of the numerical results and plots, smaller values of b result in much larger relative errors W/V and do not represent good approximations. For comparison, the relative error W/V will also be shown for $b = 1$, corresponding to a much larger $\rho_R/\rho_0 \simeq 37\%$.

In Fig. 6 we display the relative errors for several values of the polytropic index covering the range $1 < n < 2$ for all three values of the compactness and the two values of b discussed earlier. In general, the relative error W/V is smaller for larger values of b , corresponding to flat Gaussian profiles with the density at the surface approximately equal to the one in the center, thus departing from our initial approximation. This general trend was also observed for other values of b not included here.

With very few exceptions, the relative error grows to a maximum around the center and vanishes at $r = R$. A simple explanation is that, while the parameter ρ_0 was obtained using only the leading order terms in the series expansion of the field of motion around $r = 0$, the boundary conditions at $r = R$ were matched exactly.

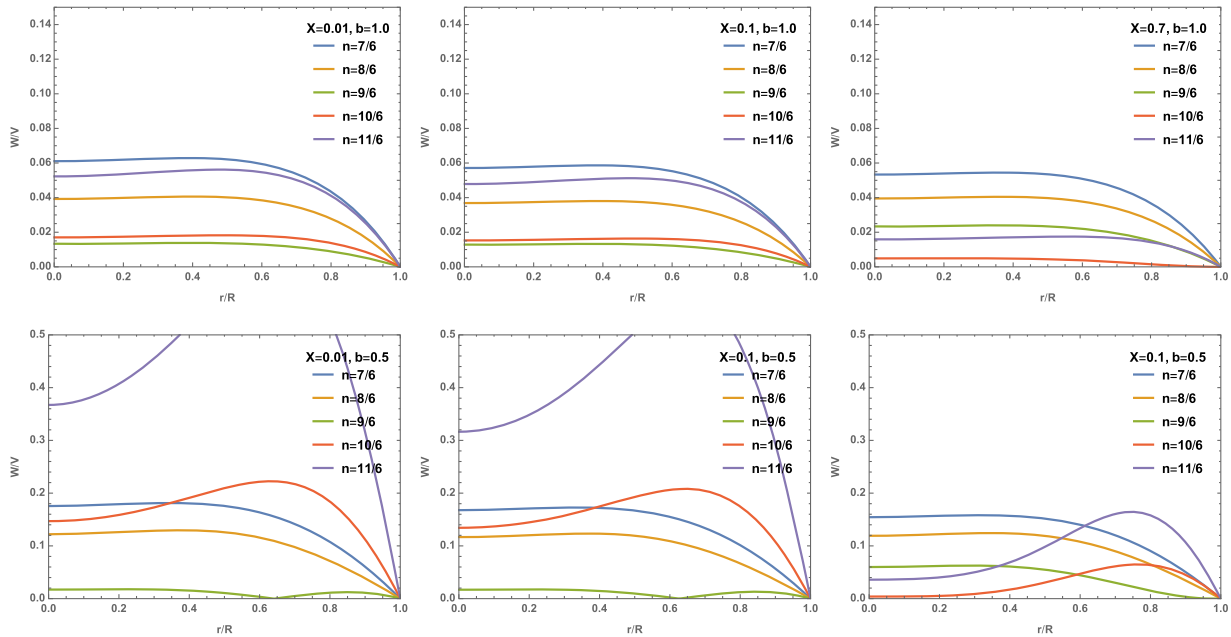


FIG. 6. Relative error for different values of the polytropic index n for $q_c = q_\Phi = 1$. Note the different ranges on the vertical axis for the top plots versus the ones in the bottom.

For a fixed width $b = 0.5$, the errors are the smallest for $n = 3/2$, at least for small and intermediate compactness. In the high compactness case, even though the relative errors are always large, they become smaller for $n = 5/3$, which signals a possible transition from $n = 3/2$ to $n = 5/3$ as the compactness increases.

The ratio M_0/M for an equation of state with $n = 3/2$ is presented in Fig. 7. Only values of $b > 0.5$ are considered because, as stated before, the relative errors become unacceptably large for smaller values of this parameter. The limit of large b is in agreement with our findings from Ref. [13], where we investigated objects with uniform densities. There it was found that the ratio $M_0/M < 1$ for $q_\Phi = 1$. In fact, this ratio is smaller than one throughout

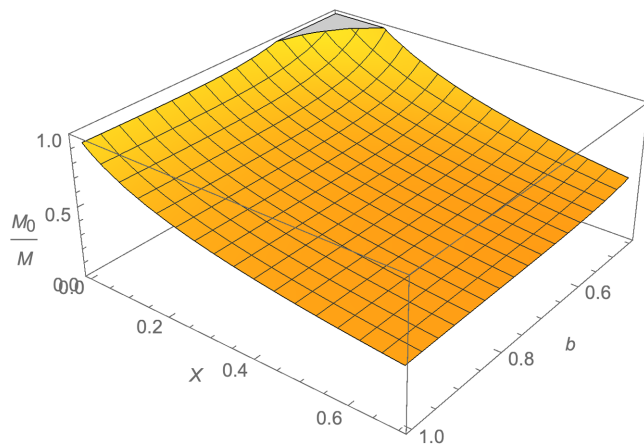


FIG. 7. Ratio M_0/M as a function of the parameters b and X for $q_c = q_\Phi = 1$ and $n = 3/2$.

most of the parameter space investigated here. The only region in which the ratio becomes larger than one is for objects of low compactness with the density peaked strongly near the center. In the low compactness limit, the ratio approaches one, as expected.

The gravitational potential from Eq. (4.11) is plotted in Fig. 8 for the three values of X considered here and for the values of n which minimize the relative errors W/V . Alongside, we also show the Newtonian potential corresponding to the same Gaussian distribution (4.1), given by

$$V_N = \begin{cases} -\frac{X[2r - \sqrt{\pi}bRe^{1/b^2} \text{Erf}(\frac{r}{bR})]}{r[2 - \sqrt{\pi}be^{1/b^2} \text{Erf}(\frac{1}{b})]}, & r \leq R \\ -\frac{G_N M}{r}, & r > R, \end{cases} \quad (4.13)$$

for which we recall that the proper mass $M_0 = M$. The plots we obtain are consistent with our earlier findings. The errors resulting from solving the equation of motion numerically are smaller for larger value of b , represented in the three bottom plots, when compared to the corresponding plots obtained for the same values of the compactness, but smaller b values. As expected, the differences between the Newtonian and the bootstrapped Newtonian potentials are larger for more compact objects and they becomes negligible as the density decreases. The Newtonian potential generally creates deeper wells for most sources except for those characterized by small values of the compactness and small values of the parameter b (in our case for $X = 0.01$ and $b = 0.5$). Considering that $M_0 = M$ in the Newtonian case, this signals that the ratio M_0/M crosses one, as also observed in Fig. 7. However, we do not show

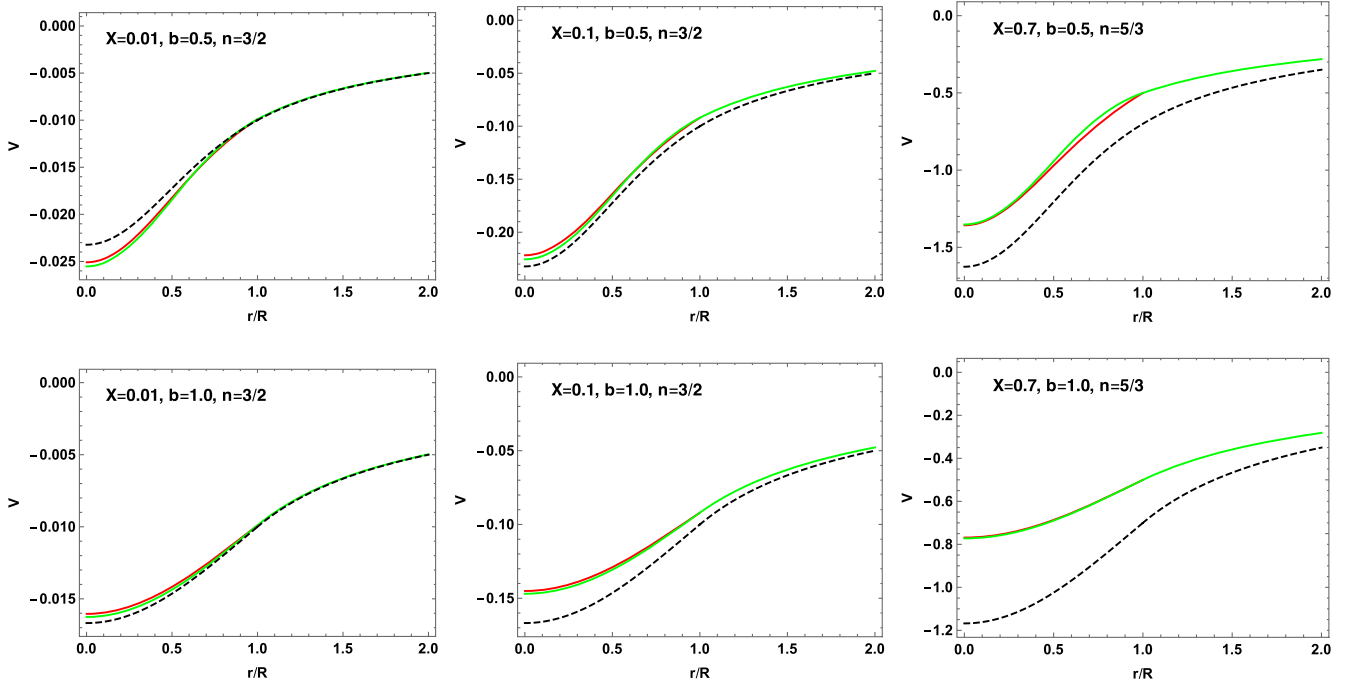


FIG. 8. Bootstrapped potentials for $q_c = q_\Phi = 1$: V_b in Eq. (4.11) (green lines) and V in Eq. (4.12) (red lines). For $X = 0.01$ and $X = 0.1$ we used $n = 3/2$, while for $X = 0.7$ we used $n = 5/3$. The dashed black lines represent the Newtonian potential V_N in Eq. (4.13) for a Gaussian matter distribution with the same b .

here that, even in this case, we could find a value of the polytropic index n slightly smaller than $n = 3/2$, for which the ratio M_0/M remains smaller than one, although we cannot be certain that the same happens for general values of X and b .

Finally, we show in Fig. 9 the ratio

$$\frac{p}{\rho} = \frac{X e^{(n-1)(1-r^2/R^2)/b^2}}{\frac{2n}{b^2} (1 + 6q_\Phi X)^{1/3} - q_c X} \quad (4.14)$$

for each of the cases presented above. For both values of b taken into consideration, this ratio increases with the compactness. What we observe is the expected behavior in both limits: while the pressure is negligible with respect to the density for objects of small compactness, the ratio becomes larger as the objects become more compact, until the two quantities are roughly of the same order of magnitude.

V. COMPARISON WITH GENERAL RELATIVITY

From the physical point of view, it is important to compare the solutions obtained in the bootstrapped Newtonian picture with similar solutions of the Tolman-Oppenheimer-Volkoff (TOV) equation [16] of general relativity, namely

$$r^2 p' = -G_N (p + \rho) (m + 4\pi r^3 p) \left(1 - \frac{2G_N m}{r}\right)^{-1}, \quad (5.1)$$

where the Bondi mass function $m = m(r)$ is given by the same expression in Eq. (3.1). It is however important to notice that the radial coordinate r in the bootstrapped Newtonian picture is associated with harmonic coordinates, and differs from the areal radius usually employed in the description of spherically symmetric systems in general relativity.⁴ Correspondingly, the expression (3.1), which defines the proper mass in the bootstrapped Newtonian case, yields the Bondi mass of the star in general relativity. The latter, computed at the star surface of radius $r = R_{\text{TOV}}$,⁵ equals the ADM mass $m(R_{\text{TOV}}) = M_{\text{TOV}}$ of the star [12].

Given a specific equation of state, the TOV equation (5.1) determines the density profile $\rho = \rho(r)$ of the compact source and can typically be solved only numerically. In order to keep our comparison straightforward, we confront numerical solutions for polytropic stars in the bootstrapped Newtonian picture, as they were obtained in Sec. III C, with solutions obtained by solving numerically the TOV equation with the same equation of state (3.2) and central density $\rho_0 = \rho(0)$. In particular, since the equation of state and ρ_0 are the same, the central pressure $p_0 = p(0)$ in the

⁴We use the same symbol r for both coordinates in order to keep the notation simpler, but a complete analysis of this important issue requires deriving an effective bootstrapped metric which is currently being investigated [17].

⁵In this section, we usually denote quantities computed in general relativity with the suffix TOV, in order to distinguish them from the analogous quantities computed in the bootstrapped Newtonian picture.

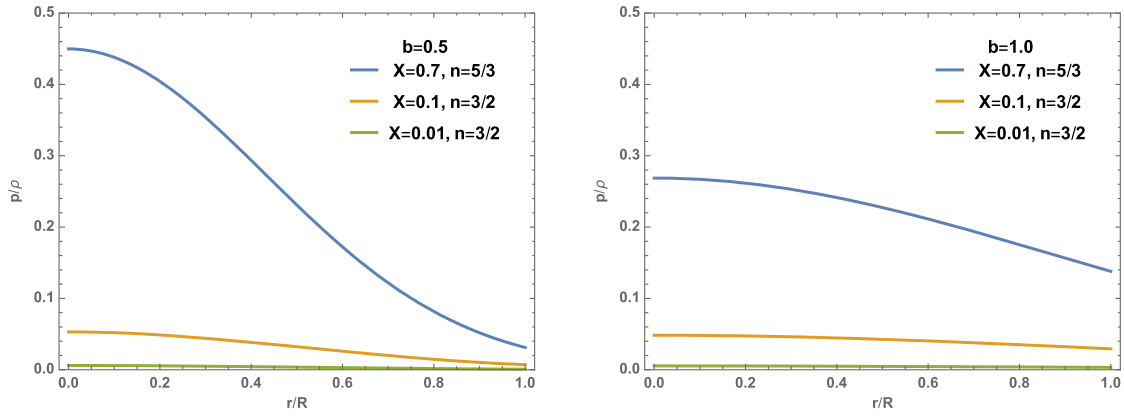


FIG. 9. Ratio of pressure to density for $q_c = q_\Phi = 1$.

TOV solution also equals the central pressure in the bootstrapped Newtonian solutions. A few cases corresponding to different values of the compactness X are shown in Fig. 10, where the pressure profiles $p = p(r)$ in the lower panels correspond to the density profiles $\rho = \rho(r)$ in the upper panels. Also note that the bootstrapped Newtonian quantities are plotted as functions of r/R , with R the corresponding star radius, whereas the TOV quantities are shown in terms of r/R_{TOV} , with R_{TOV} being the star radius obtained from solving Eq. (5.1). We remark once more that R and R_{TOV} in general differ, as we will discuss below. For exemplification purposes, we also included the lines representing the Gaussian approximation. The most

relevant numerical quantities for the plotted cases are then displayed in Table I.

We first notice that we could find general relativistic solutions throughout the entire bootstrapped Newtonian compactness range $0.1 \leq X \leq 0.7$, since the values of the corresponding TOV compactness are lower than the Buchdahl limit, $X_{\text{TOV}} < X_{\text{BL}} = 4/9$. The general relativistic density profiles are always below the curves obtained numerically in the bootstrapped picture (we will refrain from comparisons with the Gaussian approximation since in that case a certain degree of arbitrariness exists in the choice of the parameter b). This is consistent with the ratio of the masses M_{TOV}/M always being smaller than one.

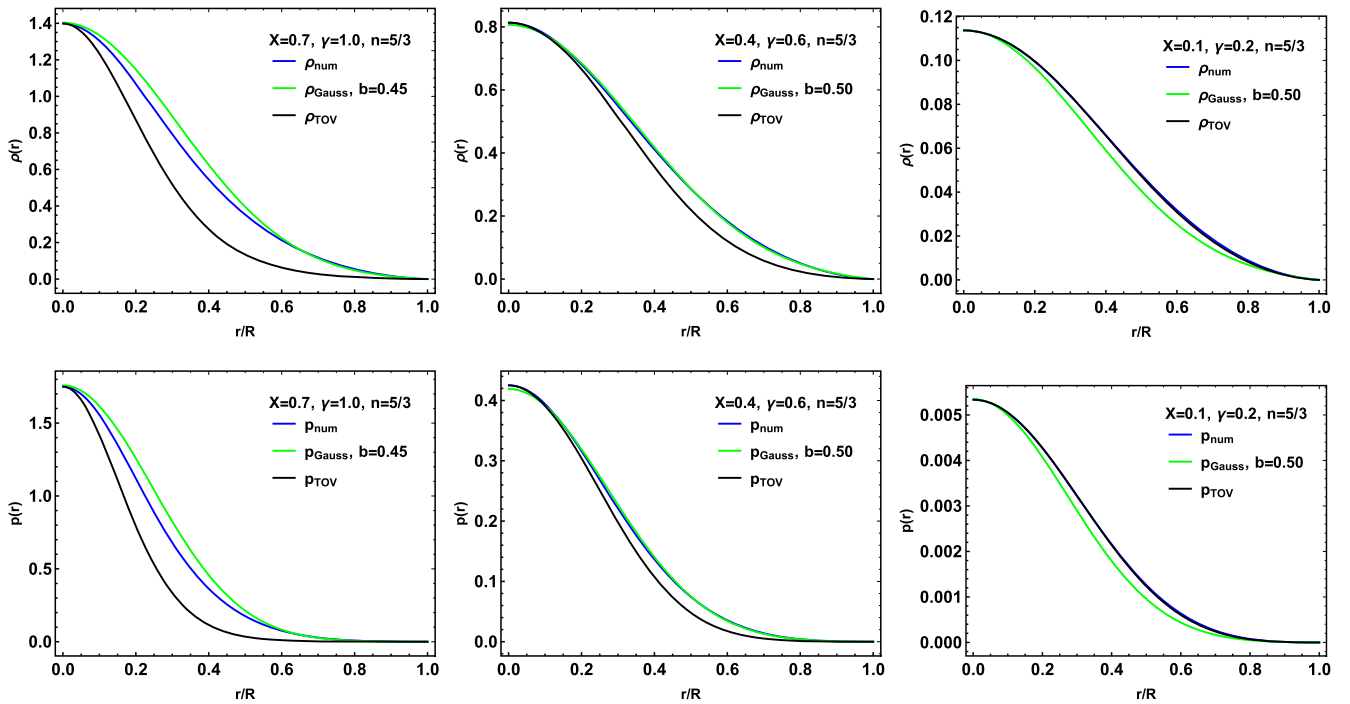


FIG. 10. Upper panels: density profiles obtained for polytropic stars by solving numerically the equation for the density (3.27) in the bootstrapped picture (blue), the Gaussian density profiles which approximate these solutions (green) and the corresponding general relativistic density profiles (black). Lower panels: pressure profiles for the same polytropic stars. For all plots $q_c = q_\Phi = 1$.

TABLE I. Comparison between bootstrapped Newtonian parameters and TOV solution for the cases in Fig. 10.

X	n	$\bar{\gamma}$	$G_N \rho_0 R^2$	$G_N p_0 R^2$	R_{TOV}/R	M_{TOV}/M	X_{TOV}	X_{TOV}/X
0.7	5/3	1.0	1.40	1.75	0.92	0.35	0.23	0.33
0.4	5/3	0.6	0.81	0.42	0.81	0.39	0.23	0.58
0.1	5/3	0.2	0.11	0.005	0.95	0.83	0.070	0.70

As the compactness X decreases, this ratio becomes closer to one and the two density profiles become virtually identical. Moreover, the radius R of a bootstrapped Newtonian star is also usually larger than the R_{TOV} of the general relativistic polytrope. The fact that $X > X_{\text{TOV}}$ means that the bootstrapped picture can allow for the existence of more compact (either smaller in size or more massive) polytropic stars than general relativity. When looking at the lower panels of Fig. 10 in comparison to the upper ones, we see that just like in the case of the density profiles, the pressure inside bootstrapped Newtonian polytropes is always larger (for high compactness values) or at least equal (for low compactness) to the pressure inside the corresponding general relativistic cases.

VI. CONCLUSIONS AND OUTLOOK

We have extended our model of bootstrapped Newtonian stars from Ref. [4] by investigating objects with nonuniform mass distribution. We assumed a polytropic equation of state to determine the relation between the density and the pressure inside the star. In order to avoid singular configurations, we imposed the condition for the first derivative of the density to vanish in the center of the star. The other boundary condition was for the density to vanish at the surface. Starting from the equation of continuity and the polytropic equation, we could rewrite the field equation in terms of the density and its derivatives. This was then solved numerically to obtain the density profile for various values of the compactness X of the star, the parameters γ and n which define the polytropic state and the coupling constants in our model (which we usually set to one for simplicity). Ideally, in order to draw general conclusions, one should scan the entire parameter space, which is a very demanding numerical task we prefer to leave for future developments. However, the numerical results presented in Sec. III C show density profiles which can be approximated by Gaussian distributions fairly accurately, therefore, we focused on these solutions next.

Starting from a Gaussian density profile, along with the polytropic equation of state, one can describe the star in terms of the width b of the distribution, the polytropic index n and the compactness X of the object. Analytic approximations can then be obtained for the gravitational potential. The accuracy of these analytic approximations was then estimated numerically in order to determine the polytropic index n compatible with such distributions. It appears that

larger values of n are favoured for larger compactness. We also compared the proper mass M_0 to the ADM mass M , and found that $M_0 < M$ throughout most of the parameter space. We recover our previous results obtained for uniform density profiles in the large b limit. There is however a small region of the parameter space where, at least for some values of the polytropic index n , the proper mass $M_0 > M$. In this regime, we also found that the bootstrapped potential creates a deeper potential well than the Newtonian one, while in all other cases the opposite occurs (see Fig. 8). The total gravitational potential energy is computed in Appendix and turns out to be negative for all solutions analyzed. Finally, pressure and density were found to have the expected behavior. In particular, their ratio increases with compactness X and with the polytropic index n , the former having a greater impact.

We also compared the density and pressure profiles for bootstrapped Newtonian, respectively general relativistic, polytropes with the same equation of state (3.2) and central density $\rho_0 = \rho(0)$. We emphasize once more that, while the Newtonian limit is obtained when the couplings q_ϕ and q_c in Eq. (2.9) are equal to zero, the bootstrapped Newtonian gravity is expected to yield the results closest to those of general relativity for $q_\phi \simeq q_c \simeq 1$, which is the case investigated here. The preliminary results obtained for these types of stars show that the bootstrapped Newtonian gravity allows for objects with larger densities (and therefore masses). At least in the relatively high compactness regime considered in Sec. V, the bootstrapped picture leads to more compact stars than those obtained by solving the TOV equation. In other words, the bootstrapped Newtonian gravity makes a significant difference in the high compactness regime because it can accommodate for the existence of more compact and massive self-gravitating stars than general relativity, given the same polytropic equation of state and central density. Of course, these more compact and massive stars are also balanced by larger pressure values. In the opposite limit of low compactness, the density profiles predicted in the bootstrapped Newtonian picture become practically identical to those of general relativity. The phenomenological differences between the two theories therefore manifest only for highly compact objects, consistently with the original motivation of accounting for the quantum nature of matter and gravity at large compactness, a task hard to tackle starting from full general relativity. A more in depth comparison of the bootstrapped Newtonian and general relativistic stars will be the subject of future work. The comparison will be extended to not only polytropes, but also to objects governed by other equations of state.

We would like to conclude by recalling that the bootstrapped description for compact self-gravitating objects was mainly developed with the purpose of investigating the corpuscular description of quantum gravity originally put forward for black holes [18–21]. In fact, the absence of a

Buchdahl limit allows for (Newtonian) horizons surrounding a matter core of large but finite compactness. It was then shown in Ref. [9] that the bootstrapped potential for uniform sources admits a description in terms of a coherent quantum state of gravitons, provided the matter source is also described by quantum physics. It will therefore be interesting to widen the survey of the parameter space for polytropic stars here initiated in light of more explicit quantum descriptions of matter.

ACKNOWLEDGMENTS

R. C. is partially supported by the INFN grant FLAG and his work has also been carried out in the framework of activities of the National Group of Mathematical Physics (GNFM, INdAM) and COST action *Cantata*. O. M. is supported by the grant Laplas VI of the Romanian National Authority for Scientific Research.

APPENDIX: GRAVITATIONAL ENERGY

The gravitational potential energy U_G in the bootstrapped picture can be estimated from the effective Hamiltonian given in Eq. (2.8), which we separate into three contributions as [4]

$$U_G = U_{BG} + U_{GG}^{in} + U_{GG}^{out}, \quad (A1)$$

where

$$U_{BG} = 4\pi \int_0^\infty r^2 dr (\rho + q_c p) V (1 - 2q_\Phi V), \quad (A2)$$

$$U_{GG}^{in} = \frac{1}{2G_N} \int_0^R r^2 dr (V'_{in})^2 (1 - 4q_\Phi V_{in}), \quad (A3)$$

$$U_{GG}^{out} = \frac{1}{2G_N} \int_R^\infty r^2 dr (V'_{out})^2 (1 - 4q_\Phi V_{out}). \quad (A4)$$

The contribution from the outer vacuum is exactly given by

$$U_{GG}^{out} = \frac{G_N M^2}{2R}, \quad (A5)$$

while the inner contributions can only be evaluated numerically within the approximations for the potential employed in the previous sections.

Since the potential V is negative and has positive slope everywhere, one can see from their expressions above that the “baryon-graviton” component U_{BG} is negative, whereas the “graviton-graviton” contributions (U_{GG}^{in} , respectively U_{GG}^{out}) are positive. As expected, the total gravitational energy is found to be negative for all solutions, regardless of the compactness of the source, the width of the gaussian, or the polytropic index. The values for each of these components for the cases discussed in Secs. III C and IV can be found in Tables II and III, respectively.

TABLE II. Gravitational potential energy for the combinations of compactness and polytropic parameters analyzed in Sec. III C.

X	$\bar{\gamma}$	n	U_{BG}/M	U_{GG}^{in}/M	U_{GG}^{out}/M	U_G/M
0.65	1	5/3	-6.9	3.6	0.21	-3.1
0.55	1	5/3	-5.8	2.8	0.15	-2.8
0.45	1	5/3	-4.7	2.0	0.10	-2.5
0.10	0.2	5/3	-1.7×10^{-2}	4.0×10^{-3}	4.0×10^{-3}	-7.6×10^{-3}
0.08	0.2	5/3	-1.3×10^{-2}	2.8×10^{-3}	3.2×10^{-3}	-7.3×10^{-3}
0.06	0.2	5/3	-1.0×10^{-2}	1.8×10^{-3}	1.8×10^{-3}	-6.4×10^{-3}
0.65	0.5	4/3	-6.6	3.8	0.21	-2.5
0.55	0.5	4/3	-5.9	3.3	0.15	-2.4
0.45	0.5	4/3	-5.2	2.8	0.10	-2.3

TABLE III. Gravitational potential energy for the combinations of Gaussian width, compactness, and polytropic index analyzed in Sec. IV.

b	X	n	U_{BG}/M	U_{GG}^{in}/M	U_{GG}^{out}/M	U_G/M
0.5	0.01	3/2	-2.1×10^{-4}	4.9×10^{-5}	5.0×10^{-5}	-1.1×10^{-4}
0.5	0.1	3/2	-2.0×10^{-2}	5.2×10^{-3}	5.0×10^{-3}	-9.7×10^{-3}
0.5	0.7	5/3	-1.5	0.52	0.25	-0.74
1.0	0.01	3/2	-1.2×10^{-4}	1.3×10^{-5}	5.0×10^{-5}	-5.5×10^{-5}
1.0	0.1	3/2	-1.1×10^{-2}	1.4×10^{-3}	5.0×10^{-3}	-4.7×10^{-3}
1.0	0.7	5/3	-0.52	0.07	0.25	-0.20

- [1] S. W. Hawking and G. F. R. Ellis, *The Large Scale Structure of Space-Time* (Cambridge University Press, Cambridge, England, 1973).
- [2] R. P. Geroch and J. H. Traschen, *Phys. Rev. D* **36**, 1017 (1987); *Conf. Proc. C* 861214, 138 (1986); H. Balasin and H. Nachbagauer, *Classical Quantum Gravity* **10**, 2271 (1993).
- [3] R. Brustein and A. J. M. Medved, *Fortschr. Phys.* **67**, 1900058 (2019); *Phys. Rev. D* **99**, 064019 (2019).
- [4] R. Casadio, M. Lenzi, and O. Micu, *Eur. Phys. J. C* **79**, 894 (2019).
- [5] R. Casadio, M. Lenzi, and O. Micu, *Phys. Rev. D* **98**, 104016 (2018).
- [6] R. Casadio, A. Giugno, and A. Giusti, *Phys. Lett. B* **763**, 337 (2016).
- [7] R. Casadio, A. Giugno, A. Giusti, and M. Lenzi, *Phys. Rev. D* **96**, 044010 (2017).
- [8] R. Carballo-Rubio, F. Di Filippo, and N. Moynihan, *J. Cosmol. Astropart. Phys.* **10** (2019) 030; S. Deser, *Gen. Relativ. Gravit.* **1**, 9 (1970); **42**, 641 (2010).
- [9] R. Casadio, M. Lenzi, and A. Ciarfella, *Phys. Rev. D* **101**, 124032 (2020).
- [10] R. Casadio and I. Kuntz, *Eur. Phys. J. C* **80**, 581 (2020).
- [11] H. A. Buchdahl, *Phys. Rev.* **116**, 1027 (1959).
- [12] R. L. Arnowitt, S. Deser, and C. W. Misner, *Phys. Rev.* **116**, 1322 (1959).
- [13] R. Casadio, O. Micu, and J. Mureika, *Mod. Phys. Lett. A* **35**, 2050172 (2020).
- [14] N. Dadhich, *Curr. Sci.* **109**, 260 (2015); J. Franklin, *Am. J. Phys.* **83**, 332 (2015).
- [15] G. P. Horendt, *Polytropes: Applications in Astrophysics and Related Fields* (Springer, Netherlands, 2004).
- [16] J. R. Oppenheimer and G. M. Volkoff, *Phys. Rev.* **55**, 374 (1939).
- [17] R. Casadio, A. Giusti, I. Kuntz, and G. Neri (to be published).
- [18] G. Dvali and C. Gomez, *J. Cosmol. Astropart. Phys.* **01** (2014) 023; arXiv:1307.7630; *Eur. Phys. J. C* **74**, 2752 (2014); *Phys. Lett. B* **719**, 419 (2013); **716**, 240 (2012); *Fortschr. Phys.* **61**, 742 (2013); G. Dvali, C. Gomez, and S. Mukhanov, arXiv:1106.5894.
- [19] A. Giusti, *Int. J. Geom. Methods Mod. Phys.* **16**, 1930001 (2019).
- [20] F. Kühnel and M. Sandstad, *Phys. Rev. D* **92**, 124028 (2015).
- [21] G. Dvali and A. Gußmann, *Nucl. Phys.* **B913**, 1001 (2016).